PNAS

More than just an eagle killer: The freshwater cyanobacterium *Aetokthonos hydrillicola* produces highly toxic dolastatin derivatives

Markus Schwark[a,1] [ID], José A. Martínez Yerena[b,c,d,1] [ID], Kristin Röhrborn[a,2] [ID], Pavel Hrouzek[d] [ID], Petra Divoká[d] [ID], Lenka Štenclová[b] [ID], Kateřina Delawská[c,d] [ID], Heike Enke[e] [ID], Christopher Vorreiter[f] [ID], Faith Wiley[g,3] [ID], Wolfgang Sippl[f] [ID], Roman Sobotka[c,d] [ID], Subhasish Saha[d,4] [ID], Susan B. Wilde[h] [ID], Jan Mareš[b,c,d,5] [ID], and Timo H. J. Niedermeyer[a,i,5] [ID]

Cyanobacteria are infamous producers of toxins. While the toxic potential of planktonic cyanobacterial blooms is well documented, the ecosystem level effects of toxigenic benthic and epiphytic cyanobacteria are an understudied threat. The freshwater epiphytic cyanobacterium *Aetokthonos hydrillicola* has recently been shown to produce the "eagle killer" neurotoxin aetokthonotoxin (AETX) causing the fatal neurological disease vacuolar myelinopathy. The disease affects a wide array of wildlife in the southeastern United States, most notably waterfowl and birds of prey, including the bald eagle. In an assay for cytotoxicity, we found the crude extract of the cyanobacterium to be much more potent than pure AETX, prompting further investigation. Here, we describe the isolation and structure elucidation of the aetokthonostatins (AESTs), linear peptides belonging to the dolastatin compound family, featuring a unique modification of the C-terminal phenylalanine-derived moiety. Using immunofluorescence microscopy and molecular modeling, we confirmed that AEST potently impacts microtubule dynamics and can bind to tubulin in a similar matter as dolastatin 10. We also show that AEST inhibits reproduction of the nematode *Caenorhabditis elegans*. Bioinformatic analysis revealed the AEST biosynthetic gene cluster encoding a nonribosomal peptide synthetase/polyketide synthase accompanied by a unique tailoring machinery. The biosynthetic activity of a specific N-terminal methyltransferase was confirmed by in vitro biochemical studies, establishing a mechanistic link between the gene cluster and its product.

cyanotoxin | cytotoxicity | aetokthonostatin | dolastatin | biosynthesis

Cyanobacteria are a prolific source of biologically active specialized metabolites (1–3). They are infamous for their potent toxins, such as the neurotoxic alkaloids anatoxins or the hepatotoxic nonribosomal peptides microcystins (4, 5). Harmful cyanobacterial blooms (mass proliferation of toxic cyanobacteria in stagnant waters) can pose a threat for ecosystem health (6). While planktic cyanobacteria have been studied intensely in the past, the effects of benthic or epiphytic cyanobacteria remain largely unknown, although their cyanotoxin repertoire is equally high, and they have been linked to numerous animal poisonings (7). Recently, a novel cyanobacterial toxin was discovered from the filamentous epiphytic cyanobacterium *Aetokthonos hydrillicola* (8). The biindole alkaloid aetokthonotoxin (AETX, Fig. 1*A*) has been found to be the cause of the disease Vacuolar Myelinopathy (VM), affecting wildlife in the southeastern United States. *A. hydrillicola* grows on submersed aquatic plants, especially the invasive *Hydrilla verticillata*, which is consumed by waterfowl, fish, and snails, which in turn are consumed by birds of prey. AETX consumption resulted in VM throughout every trophic level of this aquatic food chain (8).

Biologically active cyanobacterial specialized metabolites provide opportunities for drug substance development (1, 9, 10). Prominent examples that have advanced into clinical studies are saxitoxins as long-lasting local anesthetics (11, 12) or cryptophycins as potential antineoplastic drugs (13, 14). However, the only cyanobacterial natural products of which derivatives are clinically used to date are the dolastatins (1, 9). Linear dolastatins like dolastatin 10 are pentapeptides that contain two uncommon amino acids characteristic for the dolastatin compound family, dolaproine (Dap) and dolaisoleuine (Dil) (15). Linear dolastatins as well as structurally related peptides of cyanobacterial origin, e.g., symplostatin 1 (16) or malevamide D (17), are highly cytotoxic (low to sub-nM EC_{50}). Binding to the vinca binding site of the β1 subunit of tubulin, they interrupt microtubule assembly, resulting in cell cycle arrest in the G_2/M phase (18–20). Synthetic derivatives of dolastatin 10, monomethylauristatin E (MMAE) and monomethylauristatin F (MMAF), have been introduced into the clinic as highly cytotoxic payloads of antineoplastic antibody–drug conjugates. The

Significance

Cyanotoxins have adverse effects on ecosystems. Our understanding of their potential risk has recently been expanded by the discovery of aetokthonotoxin, produced by the cyanobacterium *Aetokthonos hydrillicola* growing on invasive plants. Via trophic transfer, it acts as a neurotoxin causing mortality in animals including top predators like bald eagles. Closer examination of *A. hydrillicola* revealed that it also produces highly toxic dolastatin derivatives. *A. hydrillicola* is the only known cultured cyanobacterium producing dolastatin derivatives, which allowed uncovering biosynthetic gene clusters of this compound family. In contrast to all other known dolastatin producers, which are marine cyanobacteria, *A. hydrillicola* thrives in freshwater reservoirs, making it a potential threat also for human health. Monitoring of the cyanobacterium and its toxins is strongly recommended.

[1]M.S. and J.A.M.Y. contributed equally to this work.

[2]Present address: Clinical Obesity Research Group, Helmholtz Institute for Metabolic, Obesity and Vascular Research, Leipzig 04103, Germany.

[3]Present address: Department of Biological Sciences, Augusta University, Augusta, GA 30912.

[4]Present address: SecondCircle, Søborg 2860, Denmark.

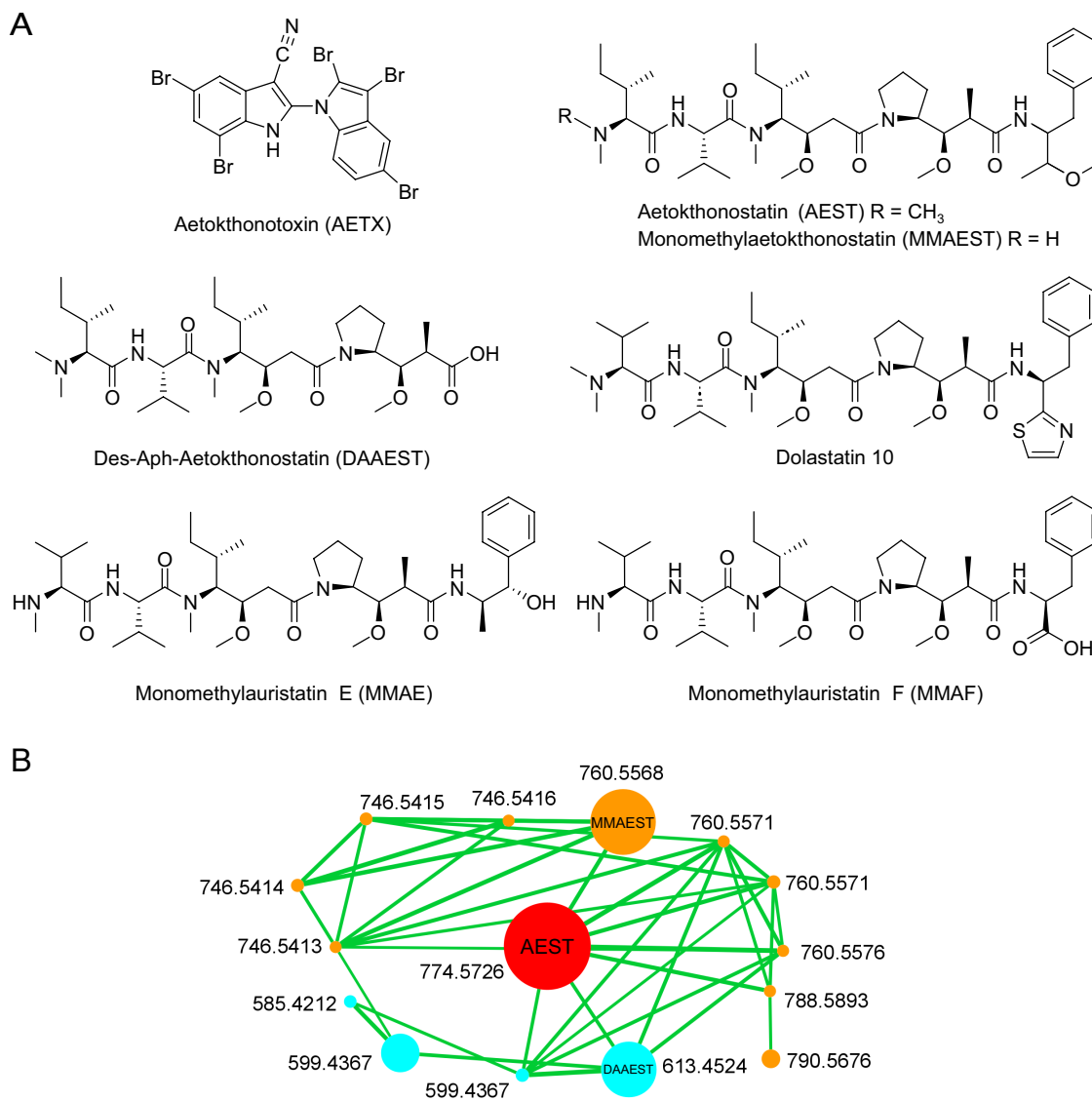[5]To whom correspondence may be addressed. Email: jan.mares@hbu.cas.cz or timo.niedermeyer@fu-berlin.de.

Fig. 1. *A. hydrillicola* produces dolastatin analogs. (*A*) Structures of AETX, AEST, MMAEST, DAAEST, as well as MMAE, MMAF and dolastatin 10. (*B*) AEST cluster in a GNPS feature-based MS/MS networking analysis of an HPLC-MS/MS analysis of an *A. hydrillicola* extract. Node size proportional to ion intensity, exact mass of [M+H]$^+$ indicated next to the respective node. Red: AEST, orange: pentapeptide AEST derivatives like MMAEST, cyan: tetrapeptide AEST derivatives like DAAEST.

first of these, brentuximab vedotin, has been approved by the US Food and Drug Administration in 2011 (9).

The dolastatins were first described from the sea hare *Dolabella auricularia* by Petitt et al. in 1987 (21). However, later studies found that sea hares acquire the dolastatins by their diet, which consists largely of cyanobacteria of the genus *Symploca*, the actual producers of these compounds (22, 23). Notably, all cytotoxic linear derivatives of dolastatin 10 known to date have been isolated from marine cyanobacteria of the genus *Symploca/Caldora* (24). Marine benthic filamentous cyanobacteria have been intensively studied as an extremely rich source of bioactive compounds (25). However, no dolastatin-producing strain has been cultured yet, hampering the elucidation of the genetic basis for the compound's biosynthesis as well as synthetic biology approaches for their modification. As well-established total synthesis routes to the dolastatins are available, ongoing research on the medicinal chemistry of dolastatins focuses on synthetic analogs (26).

Profiling the bioactivity of purified AETX and crude extracts of the cyanobacterium *A. hydrillicola*, we observed that the cytotoxicity of a crude extract of *A. hydrillicola* biomass was much stronger than the cytotoxicity of a corresponding amount of pure AETX. Thus, there had to be another compound in the extract with higher cytotoxicity than AETX. Intrigued by these results, we set out to isolate and characterize the cytotoxic compound produced by *A. hydrillicola*. Here, we present the isolation and structure elucidation of aetokthonostatin (AEST) and AEST derivatives. The AESTs are linear peptides belonging to the dolastatin compound family, featuring a yet undescribed C-terminal phenylalanine-derived building block. Immunofluorescence microscopy and molecular modeling studies suggest that AEST, like dolastatin 10, exerts its strong cytotoxicity by binding to tubulin. We show that AEST inhibits reproduction of the nematode *Caenorhabditis elegans*. Bioinformatic analysis of the *A. hydrillicola* genome revealed the biosynthetic gene cluster (BGC) of AEST, which we confirmed by biochemical experiments. Our study

highlights that the cyanobacterium *A. hydrillicola* might pose a serious threat to drinking-water supplies, as it is able to produce two specialized metabolites with pronounced toxicity.

Results and Discussion

Toxicity of *A. hydrillicola* Extract and AETX. Early investigation of a crude extract of the cyanobacterium *A. hydrillicola* for cytotoxicity showed a remarkably high activity of the extract (EC$_{50}$ 0.12 μg/mL, HeLa, *SI Appendix*, Fig. S2). Focusing on the isolation of the toxin causing VM, we assumed that the toxin causing VM would also be responsible for the extract's cytotoxicity. After isolation of AETX and testing the pure compound for cytotoxicity, to our surprise, we found that AETX is only moderately cytotoxic (EC$_{50}$ 1 μM = 0.65 μg/mL, HeLa). Quantification of the AETX content in a crude extract assayed for cytotoxicity showed that based on the determined AETX content, the extract was about fivefold more cytotoxic than expected if AETX was the sole cytotoxic compound in the extract. This suggested that another, more cytotoxic compound must be present. Indeed, time-based fractionation of the extract and subsequent cytotoxicity testing of the individual fractions revealed that not AETX but the main compound observed in the extract's HPLC chromatogram was highly cytotoxic (*SI Appendix*, Fig. S3).

Isolation and Structure Elucidation of AEST. In contrast to AETX, which is only produced by *A. hydrillicola* when the strain's cultivation medium is supplemented with bromide salts (8), we found the cytotoxic metabolite to be produced under all tested cultivation conditions. Thus, the cyanobacterium was cultivated in standard BG-11 medium to generate biomass for subsequent processing. After harvest and lyophilization, the biomass was extracted with methanol. The crude extract was fractionated using flash chromatography. Fractions were assayed for cytotoxicity, and the cytotoxic fractions were subjected to semipreparative HPLC to isolate the active compounds. We found that the main peak observed in the chromatogram (*SI Appendix*, Fig. S3) consisted of two individual compounds, which we subsequently separated using ammonium acetate buffer (pH 9) in the mobile phase.

The main compound was isolated as a white amorphous powder. High-resolution mass spectrometry suggested the molecular formula C$_{43}$H$_{76}$O$_7$N$_5$ ([M+H]$^+$ at *m/z* 774.5759). NMR analysis (*SI Appendix*, Figs. S5–S10) was complicated by a considerable signal overlap in the ^{1}H NMR spectrum, caused by the presence of two conformers in solution (ratio main to minor conformer about 3:2, *SI Appendix*, Fig. S5). Analysis of the ^{13}C and ^{1}H NMR data suggested four amide or ester carbonyls and two NH protons (NMR data see *SI Appendix*, Table S1). The presence of amide bonds was confirmed by four signals agreeing with α-carbonyl protons of amino acids, giving us confidence that the compound was a peptide. Furthermore, we observed signals of six *N*- or *O*-methyl groups. Evaluation of HSQC-DEPT, TOCSY, and COSY spectra allowed us to assemble the spin systems of the amino acid building blocks in the peptide (for a more detailed discussion, see *SI Appendix*). In addition to the amino acids valine and isoleucine, we found that the compound contains the known nonproteinogenic amino acids Dil and Dap, indicating that the compound belongs to the dolastatin compound family. The presence of Dap explained the existence of two conformers in solution, which has also been described for other compounds in the dolastatin compound family (27). We could assemble the fifth monomer as 3-methoxy-1-phenylbutan-2-amine, a yet undescribed monomer in peptide natural products, that we give the trivial name

aetophenine (Aph). The building block sequence as well as the position of the *N*- and *O*-methyl groups was deduced from an HMBC spectrum and confirmed by a ROESY spectrum. The planar structure of the compound was thus established to be *N,N*-dimethyl-Ile-Val-Dil-Dap-Aph. This sequence was supported by the fragmentation pattern in MS/MS experiments (*SI Appendix*, Fig. S11). As this planar structure differs from the structure of symplostatin 1 only by the C-terminal monomer (22), we re-recorded a ^{13}C-NMR spectrum of the compound in CD$_2$Cl$_2$ (*SI Appendix*, Fig. S6 *B* and *C*). Indeed, the NMR data of the four N-terminal monomers matched to those reported for symplostatin 1 (22), indicating that these four monomers have the same relative and absolute stereochemistries in both compounds (*SI Appendix*, Table S2). To confirm this assumption, the absolute stereochemistries of the fourth monomer, Dap, were determined by Marfey's analysis (*SI Appendix*, Fig. S12). As no reference material for Aph is available, we first tried to hydrolyze the compound and isolate Aph for subsequent VCD spectroscopic analysis. However, we found that under the strong acidic or basic conditions needed for hydrolysis, the methyl ether was hydrolyzed as well, obfuscating the original configuration. Crystallization for X-ray crystallography was not successful. The absolute configuration of Aph could thus not be determined. The structure of the compound is shown in Fig. 1*A*. This main compound produced by *A. hydrillicola* was named AEST.

The closely eluting second compound was isolated as a white amorphous powder. Its molecular formula was established as C$_{42}$H$_{74}$O$_7$N$_5$ ([M+H]$^+$ at *m/z* 760.5571), differing from AEST only by the absence of one methyl group. Analysis of the MS/MS and NMR data confirmed that, compared to AEST, this compound lacks one of the two *N*-methyl groups at the N-terminal isoleucine (*SI Appendix*, Figs. S13–S19 and Table S3). Thus, it has been identified as monomethylaetokthonostatin (MMAEST).

A third compound, isolated as a white amorphous powder, eluted earlier than AEST and MMAEST, indicating higher polarity or smaller size. Indeed, its molecular formula, C$_{32}$H$_{61}$O$_7$N$_4$ ([M+H]$^+$ at *m/z* 613.4535), suggested that it is constituted of only four amino acids. The mass difference between this compound and AEST corresponds to the C-terminal monomer of AEST, Aph. MS/MS data as well as NMR data supported the hypothesis that this monomer was missing, as no signals were observed in the aromatic region in the ^{1}H spectrum while the other signals agree with those in the spectra of AEST (*SI Appendix*, Figs. S20–S23 and Table S4), and the prominent fragment ion at *m/z* 180.13 could not be detected (*SI Appendix*, Fig. S24). This third compound was thus confirmed to be *N,N*-dimethyl-Ile-Val-Dil-Dap, des-Aph-aetokthonostatin (DAAEST).

AEST Derivatives in an *A. hydrillicola* Extract. In addition to these three isolated compounds, feature-based MS/MS networking analysis of HPLC-MS/MS data using the "Global Natural Product Social Molecular Networking" software (GNPS) (28) allowed us to detect additional AEST derivatives in an *A. hydrillicola* extract (Fig. 1*B*). These derivatives differ in the methylation pattern and the number of amino acids. Based on the ion intensity, AEST (*m/z* 774.5726) is the most abundant statin derivate in the extract, followed by its N-terminal desmethyl derivative MMAEST (*m/z* 760.5568), its des-Aph derivative DAAEST (*m/z* 613.4524), and the respective N-terminal desmethyl-des-Aph derivative (*m/z* 599.4367). Interestingly, four possible des-methyl derivatives of AEST as well as two of DAAEST could be detected as well as four derivatives of AEST and one derivative of DAAEST lacking two methyl groups. One derivative with an additional methyl group was observed (*m/z* 788.5893). While the pentapeptides represent

the major part of the AEST derivatives, significant amounts of the respective tetrapeptides are present in the extract, as well. No di- or tripeptides could be detected. The structures of most of these compounds could be deduced based on their MS/MS spectra (*SI Appendix*, Figs. S25–S42).

Bioactivity of AEST. Structure elucidation of AEST already explained the exquisite cytotoxicity of the compound: It belongs to the dolastatin compound family. Dolastatin 10 and related compounds are known for their ability to arrest cells in G_2/M phase due to binding to tubulin and disrupting its assembly to microtubules (18–20). The cytotoxicity of AEST was assessed against HeLa cells and the triple-negative breast cancer cell line MDA-MB 231 and compared to the cytotoxicity of monomethylauristatin E (MMAE) and monomethylauristatin F (MMAF), which are used as payloads in approved antibody–drug conjugates (29, 30). We found that AEST (EC_{50} 1 ± 0.2 nM) is equally potent as MMAE (EC_{50} 3 ± 0.4 nM) against HeLa cells (31). Both are about 170-fold more active than MMAF (EC_{50} 170 ± 30 nM; *SI Appendix*, Fig. S4A) against MDA-MB 231 cells (31). In HeLa cells, this effect was less distinct; AEST and MMAE were 10-fold more active (Fig. 2A).

Due to its negative charge under physiological pH conditions, auristatins possessing a carboxy group at the C-terminal monomer have lower cell permeability, explaining the lower in vitro potency of MMAF compared to MMAE (32). AEST, like MMAE, features an uncharged C terminus. Therefore, it belongs to the MMAE group of dolastatin analogs, which show higher membrane permeability and thus lower EC_{50} values. Lack of the methyl group at the N-terminal nitrogen in MMAEST does not have noticeable influence on potency against HeLa cells (EC_{50} 4 ± 0.01 nM; Fig. 2A). We found that the C-terminal monomer of AEST is not mandatory for cytotoxicity, as DAAEST is still strongly cytotoxic (EC_{50} 25 ± 1.4 nM; Fig. 2A). This finding was surprising, as it is assumed that a phenyl moiety at the C terminus is mandatory for cytotoxicity (33, 34). However, interestingly, Pettit et al. found that the methyl ester of the N-terminal tetrapeptide of dolastatin 10 was about 30-fold less cytotoxic against L1210 cells compared to dolastatin 10, although it interacted comparably with tubulin (35), agreeing well with the potency difference of AEST and DAAEST we found in this study. This indicates that the lower potency of DAAEST might not only be due to reduced uptake caused by its free carboxylic acid.

The residual survival rate was about 50% in the case of AEST even at high concentrations (Fig. 2A). This dose–response behavior is similar to that observed for MMAE (30). Interestingly, MMAEST, and even more pronounced DAAEST, had a lower residual cell viability (about 30% and 20%, resp.).

In early experiments with *C. elegans* and *Danio rerio*, we observed that the crude *A. hydrillicola* extract seemed to be more toxic than isolated AETX. Having identified AEST as a second toxin in the extract, we wondered whether it contributed to the extract's toxicity. However, in stark contrast to AETX, but in agreement with previous findings on dolastatin 15 (36), AEST showed no acute toxic effect on *C. elegans* even at high concentrations of up to 56 μM. Instead, a decrease in the nematode's reproduction rate could be observed at low concentration (EC_{50} 0.8 ± 0.2 μM, Fig. 2B). Thus, *A. hydrillicola* produces two toxins displaying different types of toxicity.

As dolastatin 10 and related compounds are well-known tubulin inhibitors binding at the vinca domain, we performed a docking study to test whether AEST can bind to tubulin in a similar fashion to known dolastatin derivatives. As the absolute configuration of the two stereocenters of Aph could not yet be determined, we

considered all four possible stereoisomers in this study. Using a crystal structure of a dolastatin analog cocrystallized with tubulin as template (Protein Data Bank ID 4X1K), we found that both AEST and MMAF can nicely be fit into the respective tubulin binding site (Fig. 2B; for a detailed discussion of the docking study, see *SI Appendix*). The carbonyl oxygen atoms of Dil and Dap form hydrogen bonds to the backbone amide NH groups of Tyr β224 and Gly β225, respectively. The carbonyl oxygen as well as the amide NH of Val form a bifocal hydrogen bond network with the side chain of Asn α329 (Fig. 2B). The charged N-terminal dimethylamino group shows electrostatic interactions with Asp β179. The C-terminal benzyl group showed different orientations in the docking poses (either buried toward Gly α225 or cation-π interaction with Arg β278). The flexibility of the C-terminal group was also observed in the molecular dynamics simulations of AEST and structurally similar cocrystalized peptides, where the C-terminal benzyl moiety is moving significantly during the simulations (*SI Appendix*, Fig. S46). This agrees with our finding that DAAEST, lacking the Aph unit, is still strongly cytotoxic. Also, it suggests that the absolute configuration of the stereocenters of Aph is not important for tubulin binding.

We subsequently confirmed inhibition of tubulin polymerization by AEST experimentally by immunofluorescence staining (Fig. 2D). Both AEST and MMAF were assessed in this assay. As expected, the tubulin network appeared affected by AEST at a concentration well below the EC_{50} value (observable effect at 0.1 nM) and proceeding toward higher concentrations, while for MMAF, the tubulin network morphology was comparable to untreated control cells at concentrations around 1 nM. Similar data were obtained with MDA-MB 231 cells, with the activity windows shifted toward higher concentrations (*SI Appendix*, Fig. S4B).

Biosynthesis of AEST. Surprisingly, although dolastatin 10 derivatives have been part of the first and to date only approved drugs based on cyanobacterial specialized metabolites, their biosynthesis has not yet been studied. In the genome of *A. hydrillicola* Thurmond2011, we located a 36.94 kbp long nonribosomal peptide synthetase/polyketide synthase (NRPS/PKS) gene cluster (GenBank accession number ON840103) consisting of twelve genes with deduced functions in AEST biosynthesis (Fig. 3A and *SI Appendix*, Table S5). It was found in the middle of a 472 kbp long contig of clearly cyanobacterial origin. The putative *aes* BGC included four NRPS genes (*aesA*, *C*, *F*, and *G*), harboring altogether five amino acid incorporating modules (Fig. 3B). The predicted substrate specificities of all the respective adenylation domains (*SI Appendix*, Table S6) and the occurrence of two additional *N*-methyltransferase domains agreed with the observed amino acids in AEST. Specifically, a starter unit of AesF was predicted to activate isoleucine and methylate it to form an N-terminal *N*-methylisoleucine residue, followed by the incorporation of valine and another *N*-methylisoleucine by two downstream NRPS modules of AesG. According to our prediction, the subsequent biosynthetic steps are not fully colinear with the arrangement of *aes* genes, analogously to other reported NRPS/PKS biosyntheses (37–39). We suggest that in the next step, the PKS enzyme AesJ, which contains a ketoreductase (KR) domain, accomplishes elongation of the nascent acyl chain by a reduced malonyl (*SI Appendix*, Table S7), as present in Dil. Enzymes encoded in a cassette of genes *aesA-D* likely accomplish the remaining steps in the formation of the AEST backbone. AesA was predicted to incorporate proline, followed by another elongating and ketoreducing PKS (AesB) responsible for incorporation of the reduced malonyl residue of Dap (*SI Appendix*, Table S7). The predicted stereo-configuration of ketide substrates of the KR
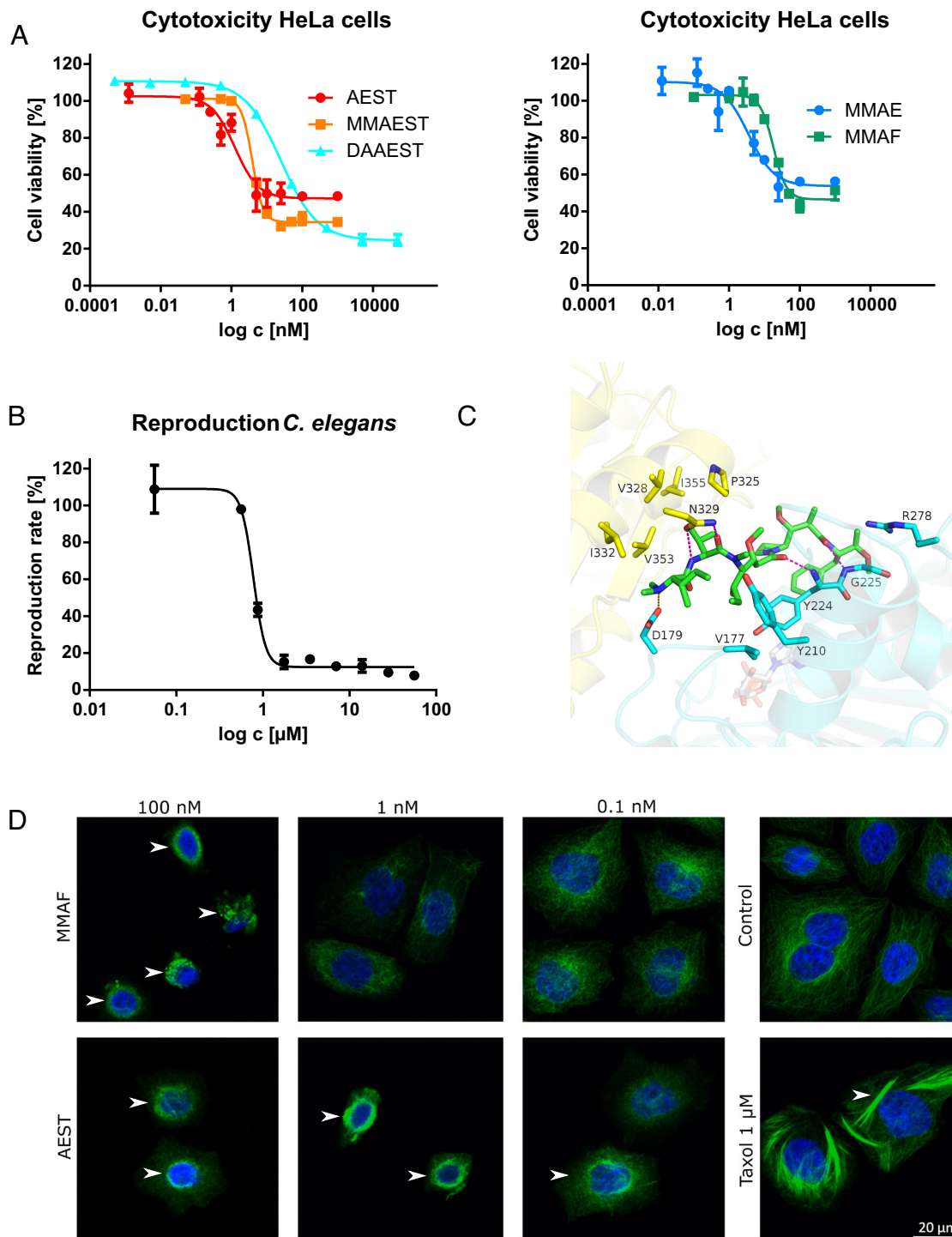
Fig. 2. AEST is a cytotoxic tubulin binder. (*A*) Cytotoxicity of AEST (EC$_{50}$ 1 ± 0.2 nM), MMAEST (EC$_{50}$ 4 ± 0.2 nM), DAAEST (EC$_{50}$ 25 ± 1.4 nM), MMAE (EC$_{50}$ 3 ± 0.4 nM), and MMAF (EC$_{50}$ 18 ± 0.7 nM) on HeLa cells (n = 3). Data are represented as average ± SEM. (*B*) Decrease of the reproduction rate of *C. elegans* treated with AEST (EC$_{50}$ 0.8 ± 0.2 μM, n = 3). Data are represented as average ± SEM. (*C*) Predicted binding of AEST (Aph as 2*S*,3*R*) to tubulin; tubulin α-subunit of one heterodimer visualized as yellow cartoon, the β-subunit of its neighboring heterodimer in cyan. Interacting binding site residues represented as sticks colored the same way. Magenta: hydrogen bonds, orange: salt bridges, red: cation–π interactions. Cofactor GDP shown as white, transparent sticks. (*D*) Immunofluorescence microscopy of HeLa cells showing the effect of AEST and MMAF on the tubulin network (green); nuclei stained with DAPI (blue). Arrows indicate tubulin network depolymerization after AEST and MMAF treatment (disruption of thread-like organization of microtubules). Taxol treatment, used as technical control to show detectability of tubulin interactions, results in tubulin stabilization and bundle formation typical for taxol.

domains embedded in AesJ and AesB match the configuration observed in the produced compounds (Fig. 1 and *SI Appendix*, Fig. S49 and Table S7). The last amino acid, phenylalanine, was predicted to be incorporated by AesC, and elongated by two additional carbons by the activity of the terminal PKS (AesD). AesD further included a thioesterase domain, which was predicted

to catalyze the cleavage of the acyl intermediate from the NRPS/PKS megasynthetase. The remaining biosynthetic step(s) leading to formation of the Aph residue of AEST were partly obscure. Such modification would likely involve a decarboxylation and reduction step (Fig. 3*B*); however, these enzymatic activities are not found in AesD. We hypothesize these reactions could be achieved by a
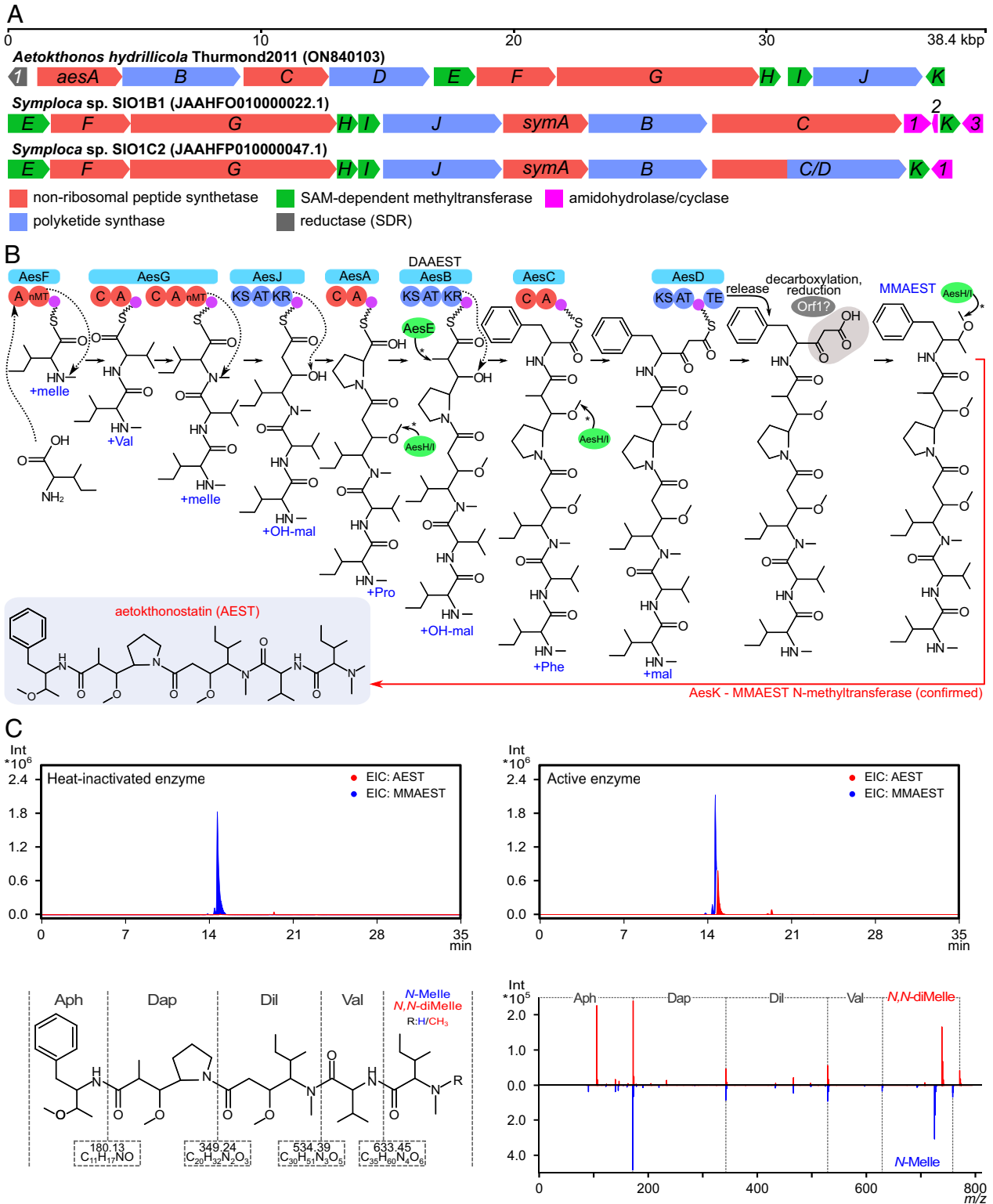
Fig. 3. AESTs are synthesized via an NRPS/PKS pathway. (*A*) Organization of the AEST BGC compared to homologous putative BGCs of members of the dolastatin compound family found in publicly available metagenome-assembled genomes of environmental marine *Symploca* sp. The *aes* orthologs identified in *Symploca* sp. are labeled *symA–K* as they presumably do not code for AESTs but rather symplostatins. The order of *symA–K* genes is collinear with the proposed biosynthesis of the symplostatin backbone scaffold. (*B*) Scheme of the predicted biosynthetic assembly of AEST. The chronology of the tailoring methylation reactions catalyzed by AesE, H, and I (marked with asterisks) is unknown; the reactions are depicted at their first theoretically suitable substrate. The specific target moieties of AesH/I (the Dil/Dap/Aph OH groups) remain to be assigned experimentally. The proposed decarboxylation/reduction of the C-terminal AEST residue (gray box) was not fully explained by bioinformatic analysis. The N-terminal methylation (red arrow) of MMAEST was reconstituted by in vitro enzymatic activity of AesK. (*C*) HPLC-HRMS/MS analysis (extracted ion chromatograms) of AEST (red) in reaction mixtures of MMAEST (blue) incubated with heat-inactivated or fresh Strep-AesK (*Top Left/Right*) show that the inactivated enzyme had no effect on the substrate while the fresh Strep-AesK methylated MMAEST. MMAEST and AEST differ only in the degree of methylation of the N-terminal Ile (*Bottom Left*). Comparison of the MS/MS spectra of MMAEST and the product of the fresh enzyme reaction (*Bottom Right*) shows that AesK methylated the N terminus of MMAEST, producing AEST. Abbreviations: AEST, aetokthonostatin; Aph, aetophenine; BGC, biosynthetic gene cluster; Dap, Dolaproine; Dil, Dolaisoleuine; mal, malonyl-CoA; MMAEST, monomethylaetokthonostatin; *N,N*-di-Melle, *N,N*-dimethylisoleucine; OH-mal, hydroxymalonyl-CoA; SAM, *S*-adenosylmethionine; SDR, short-chain dehydrogenase/reductase.

putative short-chain dehydrogenase/reductase (SDR) encoded by a gene (*orf1*) located at the 5′ terminus of the BGC.

The production of minor amounts of a C-terminally truncated NRPS product (DAAEST) could not be explained by our bioinformatics analyses. However, similar cases of partial premature chain termination and release of truncated peptides have been previously reported for other compounds such as the cyanobacterial linear pentapeptide microginins (40). Spontaneous release of NRPS/PKS intermediates has also been demonstrated experimentally, e.g., for bacillaene (41). Furthermore, the last module involved in DAAEST biosynthesis, AesB, ends with a KR domain (Fig. 3*B*). Since SDR domains such as KRs are among known alternative chain-release catalysts in NRPS pathways (42), one could speculate that DAAEST is released by the KR domain of AesB.

In addition to the NRPS/PKS genes, the BGC contained four genes (*aesE, H, I,* and *K*) annotated as class I S-adenosylmethionine (SAM)-dependent methyltransferases (MTs). This observation was in line with multiple methylations found in AEST, specifically the second *N*-methylation of the N-terminal isoleucine, *O*-methylation of hydroxyl groups of the Dil, Dap, and Aph residues, and an additional *C*-methyl group at C7 of AEST. As all four MTs were coded by standalone genes, it was impossible to conclusively infer their target atoms in AEST and the precise chronology of their activity in AEST tailoring—the methylation could occur at the nascent acyl chain or ex post after cleavage of the intermediate from the NRPS/PKS assembly line. We hypothesized that AesE could more likely catalyze the introduction of C7 methyl of AEST, as its closest functionally annotated hit in MIBiG was the *C-C* methyltranserase GphF (*SI Appendix,* Table S5) from the gephyronic acid biosynthetic pathway (43), and it clustered with other C-MTs in our phylogenetic analysis (*SI Appendix,* Fig. S50).

To provide a mechanistic link between the hypothetical *aes* BGC and its putative product, the three MTs AesH, I, and K were heterologously expressed in *Escherichia coli* (*SI Appendix,* Figs. S51 and S52) and subsequently used in in vitro enzymatic assays to elucidate if any of them is involved in the biosynthesis of the *N,N*-dimethylamino group at the N terminus of AEST. To test this hypothesis, aliquots containing the individual MTs and SAM were incubated with the monomethylated, putative late-stage AEST biosynthetic intermediate MMAEST as well as with its synthetic analogue MMAF. MMAF was used as an appropriate alternative substrate to test the specificity of the enzymes, as it likewise possesses a single methylation on the N-terminal residue, in this case *N*-methylvaline.

We detected no modification of the two substrates in the assays with Strep-AesH and Strep-AesI (*SI Appendix,* Figs. S53–S54). However, in the assay with Strep-AesK, we detected the formation of significant amounts of products at *m/z* 760.05, matching with the mass of AEST, in the assay containing MMAEST (Fig. 3*C*), and at *m/z* 746.05 (matching with auristatin F) in the assay containing MMAF (*SI Appendix,* Fig. S55). In both cases, the detected product matched the expected molecular mass corresponding to a single methylation of the provided substrate. HRMS/MS analysis showed that this methylation, as expected, had occurred at the N terminus of the respective substrates. Indeed, the MS/MS spectrum of the reaction product of MMAEST was identical to the MS/MS spectrum of AEST, proving that this compound was formed. (Fig. 3*C* and *SI Appendix,* Fig. S56). We suggest that MMAEST is the true substrate of AesK, as we found AesK unable to methylate the N-terminal amino acids of MMAEST, *N*-methylisoleucine, or MMAF, *N*-methylvaline, when provided as monomeric substrates (*SI Appendix,* Fig. S57).

As AesK only methylates the N terminus of both late-stage biosynthesis analogs, we could confirm its predicted role as the last

enzyme of the AEST biosynthetic pathway (Fig. 3 *B* and *C*), demonstrating that the *aes* cluster indeed is responsible for the biosynthesis of AEST. This finding provides additional experimental proof for the cyanobacterial origin of dolastatins (44, 45), offering a cultured and genome-sequenced strain for further laboratory studies. A subsequent search in bioinformatic databases identified highly homologous BGCs in metagenomic assemblies of tropical marine cyanobacteria of the genus *Symploca* (*SI Appendix,* Table S8), from which several dolastatin analogs (e.g., symplostatins) were isolated previously (16, 17, 22, 46). Interestingly, in contrast to the noncolinear arrangement of genes observed in the AEST BGC, the genes in these BGCs from *Symploca* are arranged colinearly with the statin biosynthesis (Fig. 3*A*).

It was intriguing to see that AesK exhibited sufficient substrate specificity to avoid methylation of monomeric *N*-methylisoleucine and *N*-methylvaline, while it was capable to efficiently methylate MMAF, a synthetic dolastatin analog used in antibody–drug conjugate anticancer therapy (47). AesK was originally predicted to be an *O*-MT using automatic bioinformatics tools and phylogenetic analysis (*SI Appendix,* Fig. S50). The substrate specificity of MTs associated with NRPS/PKS clusters offers an example of convergent functional evolution that leads to unexpected enzymatic capabilities (48). Future in-depth studies of AEST biosynthesis, especially the formation of the unique Aph residue, may broaden our knowledge of the cyanobacterial biosynthetic capabilities and be valuable in synthetic biology and medical biotechnology.

Materials and Methods Summary

Full experimental details as well as additional discussions and references for the chemical, biological, and computational methods can be found in *SI Appendix.*

Chemistry. NMR data were recorded on an Agilent/Varian VNMRS 600 MHz spectrometer (5 mm cryoprobe, DMSO-d$_6$). HRESIMS[2] data were acquired on a Q Exactive Plus mass spectrometer coupled to an UltiMate 3000 HPLC system (Thermo Fisher Scientific). Lyophilized cyanobacteria biomass was homogenized, and extracted three times using methanol/H$_2$O mixtures (50/50, 80/20, 100 % v/v; sonication, agitation, centrifugation, collection, and drying of the combined supernatants). The extract was dry-loaded (Celite) for flash chromatography with an ACN-H$_2$O gradient (5 to 100% in 25 min, RP-18 cartridge). Cytotoxic fractions were submitted to RP-HPLC (UltiMate 3000, Phenomenex Luna C18 5 μm, 250 × 10 mm, 6.3 mL/min, ACN-H$_2$O with 10 mM ammonium acetate, pH 9, linear gradient 60 to 85% in 15 min). The absolute configuration of Dap was determined using Marfey's method.

Biology. *A. hydrillicola* was cultivated in BG11 medium (28 °C, av. light intensity 35 μEm^{-2}s^{-1}, 5% CO$_2$) and continuously harvested. HeLa cells were cultured in Dulbecco's modified Eagle medium low glucose supplemented with 10% fetal bovine serum and 2 mM glutamine solution at 37 °C (humidified incubator, 5% CO$_2$). A sulforhodamine B assay was used to evaluate cytotoxicity (2 to 3 triplicates, 96-well plates, 10,000 cells per well). After incubation, staining, washing steps, and photometric read-out, the IC$_{50}$ was determined by nonlinear regression analysis. For immunofluorescence microscopy, HeLa and MDA-MB231 cells were grown in 6-well plates on coated coverslips. As positive technical control, 1 μM taxol was used. After treatment, fixation, staining with formalin, and permeabilization with Triton X-100, the cells were incubated with alpha-tubulin mouse monoclonal antibody, Nuc Blue™ Fixed Cell Stain solution, and Alexa Fluor 488 Rabbit Anti-Mouse IgG Secondary Antibody. After attaching the coverslips to a slide, images were acquired with a laser scanning confocal microscope. *C. elegans* were cultured at 22 °C in petri dishes on NGM agar seeded with *E. coli* OP50. Synchronous populations were obtained by treating gravid worms with 5M NaOH and 5% NaOCl, centrifugation of the lysate, and enrichment of the eggs by density gradient centrifugation (sucrose solution/water). The upper layer was transferred into sterile water (1:3) and centrifuged. The eggs were allowed to hatch in M9 buffer. For the reproduction assay, a 24-well plate was prepared with NGM agar and an *E. coli*

OP50 solution and incubated. After addition of the test compound solutions and preincubation, three age synchronized L4 larvae were placed in each well. After 72 h, the total number of healthy adult worms were counted, and the IC_{50} was determined by nonlinear regression analysis. The recombinant MTs were codon optimized and transformed in *E. coli* BL21(DE3) cells using an in-house pET-28a-derived vector with N-terminal StrepII-tag. To produce the enzymes, the *E. coli* was grown in autoinducible LB broth medium with kanamycin. After lysis and sonication, the soluble strep-tagged proteins were purified by affinity chromatography (Strep-Tactin Superflow high-capacity resin). Purity of the proteins was confirmed by SDS-PAGE. The activity of the MTs was tested in triplicates, with heat-denatured enzyme and blank (no enzyme) as negative controls, as follows: 100 µM of the substrate and 3 µM of the enzyme were incubated for 3 h at 28 °C in 100 µL assay buffer containing 100 mM Tris–HCl, 150 mM NaCl, 5 mM $MgCl_2$, 1 mM EDTA, 1 mM DTT, and 1 mM SAM. The reaction was quenched with methanol, and the supernatant obtained by centrifugation was analyzed using HPLC-MS.

Computational Methods. GNPS Molecular Networking Analysis was conducted on HPLC-MS data as described in *SI Appendix*. The previously published genome assembly of *A. hydrillicola* Thurmond2011 was improved in terms of completeness and contiguity by additional sequencing using Illumina MiSeq and Oxford Nanopore MinION, followed by reassembly of all available data (GenBank accession JAALHA020000000.2). The genome assembly was analyzed using antiSMASH v 6.0, and putative NRPS/PKS clusters were further investigated. Substrate specificity of A-domains was predicted using the Stachelhaus code; specificity of PKS AT domains and MT domains was assigned using dedicated pHMM analyses, both available through antiSMASH. A phylogenetic tree (Maximum Likelihood, GAMMA LG model, 1,000 bootstrap iterations) of MT domains was reconstructed using an alignment of bacterial MTs with known function and MTs mined from the BGCs analyzed in this study. Stereoconfiguration of PKS KR domain substrates was predicted based on an alignment of bacterial KR domains of various types together with KR domains encoded in the aes gene cluster, using an analysis of conserved residues within the active site groove. Molecular docking was carried out using four crystal structures of tubulin retrieved from the Protein Data Bank (PDB IDs 4X1I, 4X1K, 4X1Y, 4X20). The protein chains involved in forming the binding pocket were prepared using Schrödinger's Protein Preparation Wizard. Ligprep and Confgen were used to prepare the structures of respective cocrystallized inhibitors as well as AEST and MMAF for docking. All peptides were docked using Glide in Standard-Precision-Peptide mode and utilizing a core constraint

for docking pose restriction. Molecular dynamics simulations were carried out using Amber 18. The preparation steps for all protein–ligand complexes included partial charge assignments, parameterization according to selected force fields, complex solvation, and system neutralization. Prior to the actual production phase comprising 50 ns of MD simulation, each system underwent two stages of energy minimization as well as a heating and a pressure equilibration step.

Author affiliations: ªInstitute of Pharmacy, Pharmacognosy, Martin-Luther-University Halle-Wittenberg, Halle (Saale) 06120, Germany; ᵇBiology Centre of the Czech Academy of Sciences, Institute of Hydrobiology, České Budějovice 37005, Czech Republic; ᶜFaculty of Science, University of South Bohemia, České Budějovice 37005, Czech Republic; ᵈCentre Algatech, Institute of Microbiology of the Czech Academy of Sciences, Třeboň 37901, Czech Republic; ᵉSimris Biologics GmbH, Berlin 12489, Germany; ᶠInstitute of Pharmacy, Medicinal Chemistry, Martin-Luther-University Halle-Wittenberg, Halle (Saale) 06120, Germany; ᵍMarine Biotoxins Program, Center for Coastal Environmental Health and Biomolecular Research, National Oceanic and Atmospheric Administration/National Ocean Service, Charleston, SC 29412; ʰWarnell School of Forestry and Natural Resources, Fisheries and Wildlife, University of Georgia, Athens, GA 30602; and ⁱInstitute of Pharmacy, Pharmaceutical Biology, Free University of Berlin, Berlin 14195, Germany

Preprint: A preprint of this work has been uploaded to bioRxiv (bioRxiv 2023.04.12.536103).

Author contributions: M.S., J.A.M.Y., P.H., J.M., and T.H.J.N. designed research; M.S., J.A.M.Y., K.R., P.H., P.D., L.Š., K.D., H.E., C.V., F.W., R.S., S.S., J.M., and T.H.J.N. performed research; M.S., J.A.M.Y., K.R., P.H., P.D., L.Š., K.D., C.V., F.W., W.S., R.S., S.B.W., J.M., and T.H.J.N. analyzed data; and M.S., J.A.M.Y., J.M., and T.H.J.N. wrote the paper.

Competing interest statement: T.H.J.N. serves as scientific advisor in the advisory board of Simris Biologics GmbH. H.E. is CSO of Simris Biologics GmbH. The company did not have any influence on data evaluation or presentation. The other authors do not declare any competing interests.

This article is a PNAS Direct Submission.

1. T. Niedermeyer, M. Brönstrup, "Natural product drug discovery from microalgae" in *Microalgal Biotechnology: Integration and Economy*, W. Posten, Ed. (de Gruyter, 2012), pp. 169–200.
2. K. Tidgewell, B. R. Clark, W. H. Gerwick, "The natural products chemistry of cyanobacteria" in *Comprehensive Natural Products II*, H.-W. Liu, L. Mander, Eds. (Elsevier, 2010), pp. 141–188.
3. J. K. Nunnery, E. Mevers, W. H. Gerwick, Biologically active secondary metabolites from marine cyanobacteria. *Curr. Opin. Biotechnol.* **21**, 787–793 (2010).
4. H. K. Hudnell, Ed., *Cyanobacterial Harmful Algal Blooms: State of the Science and Research Needs* (Springer, 2008).
5. I. Chorus, J. Bartram, Eds., *Toxic Cyanobacteria in Water: A Guide to their Public Health Consequences, Monitoring, and Management* (CRC Press, 2021).
6. J. M. O'Neil, T. W. Davis, M. A. Burford, C. J. Gobler, The rise of harmful cyanobacteria blooms: The potential roles of eutrophication and climate change. *Harmful Algae* **14**, 313–334 (2012).
7. S. A. Wood *et al.*, Toxic benthic freshwater cyanobacterial proliferations: Challenges and solutions for enhancing knowledge and improving monitoring and mitigation. *Freshw. Biol.* **65**, 1824–1842 (2020).
8. S. Breinlinger *et al.*, Hunting the eagle killer: A cyanobacterial neurotoxin causes vacuolar myelinopathy. *Science* **371**, eaax9050 (2021).
9. D. J. Newman, G. M. Cragg, Marine-sourced anti-cancer and cancer pain control agents in clinical and late preclinical development. *Mar. Drugs* **12**, 255–278 (2014).
10. L. A. Salvador-Reyes, H. Luesch, Biological targets and mechanisms of action of natural products from marine cyanobacteria. *Nat. Prod. Rep.* **32**, 478–503 (2015).
11. L. E. Llewellyn, Saxitoxin, a toxic marine natural product that targets a multitude of receptors. *Nat. Prod. Rep.* **23**, 200–222 (2006).
12. A. P. Thottumkara, W. H. Parsons, J. Du Bois, Saxitoxin. *Angew. Chem. Int. Ed. Engl.* **53**, 5760–5784 (2014).
13. M. Eggen, G. I. Georg, The cryptophycins: Their synthesis and anticancer activity. *Med. Res. Rev.* **22**, 85–101 (2002).
14. J. Rohr, Cryptophycin anticancer drugs revisited. *ACS Chem. Biol.* **1**, 747–750 (2006).
15. R. Bai, G. R. Pettit, E. Hamel, Dolastatin 10, a powerful cytostatic peptide derived from a marine animal. *Biochem. Pharmacol.* **39**, 1941–1949 (1990).
16. G. G. Harrigan *et al.*, Symplostatin 1: A dolastatin 10 analogue from the marine cyanobacterium *Symploca hydnoides*. *J. Nat. Prod.* **61**, 1075–1077 (1998).
17. F. D. Horgen, E. B. Kazmierski, H. E. Westenburg, W. Y. Yoshida, P. J. Scheuer, Malevamide D: Isolation and structure determination of an isodolastatin H analogue from the marine cyanobacterium Symploca hydnoides. *J. Nat. Prod.* **65**, 487–491 (2002).
18. M. Beckwith, W. J. Urba, D. L. Longo, Growth inhibition of human lymphoma cell lines by the marine products, dolastatins 10 and 15. *J. Nat. Cancer Inst.* **85**, 483–488 (1993).
19. A. Cormier, M. Marchand, R. B. G. Ravelli, M. Knossow, B. Gigant, Structural insight into the inhibition of tubulin by vinca domain peptide ligands. *EMBO Rep.* **9**, 1101–1106 (2008).
20. R. L. Bai, G. R. Pettit, E. Hamel, Binding of dolastatin 10 to tubulin at a distinct site for peptide antimitotic agents near the exchangeable nucleotide and vinca alkaloid sites. *J. Biol. Chem.* **265**, 17141–17149 (1990).
21. G. R. Pettit *et al.*, The isolation and structure of a remarkable marine animal antineoplastic constituent: Dolastatin 10. *J. Am. Chem. Soc.* **109**, 6883–6885 (1987).
22. H. Luesch, R. E. Moore, V. J. Paul, S. L. Mooberry, T. H. Corbett, Isolation of dolastatin 10 from the marine cyanobacterium Symploca species VP642 and total stereochemistry and biological evaluation of its analogue symplostatin 1. *J. Nat. Prod.* **64**, 907–910 (2001).
23. H. Luesch, G. G. Harrigan, G. Goetz, F. D. Horgen, The cyanobacterial origin of potent anticancer agents originally isolated from sea hares. *Curr. Med. Chem.* **9**, 1791–1806 (2002).
24. N. Engene, A. Tronholm, L. A. Salvador-Reyes, H. Luesch, V. J. Paul, Caldora penicillata gen. nov., comb. nov. (Cyanobacteria), a pantropical marine species with biomedical relevance. *J. Phycol.* **51**, 670–681 (2015).
25. T. Leão *et al.*, A multi-omics characterization of the natural product potential of tropical filamentous marine cyanobacteria. *Mar. Drugs* **19**, 20 (2021).
26. A. Maderna, C. A. Leverett, Recent advances in the development of new auristatins: Structural modifications and application in antibody drug conjugates. *Mol. Pharmaceut.* **12**, 1798–1812 (2015).
27. M. P. Johansson, H. Maaheimo, F. S. Ekholm, New insight on the structural features of the cytotoxic auristatins MMAE and MMAF revealed by combined NMR spectroscopy and quantum chemical modelling. *Sci. Rep.* **7**, 15920 (2017).
28. L.-F. Nothias *et al.*, Feature-based molecular networking in the GNPS analysis environment. *Nat. Methods* **17**, 905–908 (2020).
29. S. B. Singh, Discovery and development of dolastatin 10-derived antibody drug conjugate anticancer drugs. *J. Nat. Prod.* **85**, 666–687 (2022).

30. S. O. Doronina et al., Development of potent monoclonal antibody auristatin conjugates for cancer therapy. *Nat. Biotechnol.* **21**, 778–784 (2003).
31. S. O. Doronina et al., Enhanced activity of monomethylauristatin F through monoclonal antibody delivery: Effects of linker technology on efficacy and toxicity. *Bioconjug. Chem.* **17**, 114–124 (2006).
32. P. N. Moquist et al., Novel auristatins with high bystander and cytotoxic activities in drug efflux-positive tumor models. *Mol. Cancer Ther.* **20**, 320–328 (2021).
33. K. Miyazaki et al., Synthesis and antitumor activity of novel dolastatin 10 analogs. *Chem. Pharm. Bull.* **43**, 1706–1718 (1995).
34. J. Poncet et al., Synthesis and biological activity of chimeric structures derived from the cytotoxic natural compounds dolastatin 10 and dolastatin 15. *J. Med. Chem.* **41**, 1524–1530 (1998).
35. G. R. Pettit et al., Antineoplastic agents 365. Dolastatin 10 SAR probes. *Anticancer Drug Des.* **13**, 243–277 (1998).
36. I. Zubovych, T. Doundoulakis, P. G. Harran, M. G. Roth, A missense mutation in Caenorhabditis elegans prohibitin 2 confers an atypical multidrug resistance. *Proc. Natl. Acad. Sci. U.S.A.* **103**, 15523–15528 (2006).
37. N. Traitcheva, H. Jenke-Kodama, J. He, E. Dittmann, C. Hertweck, Non-colinear polyketide biosynthesis in the aureothin and neoaureothin pathways: An evolutionary perspective. *Chembiochem* **8**, 1841–1849 (2007).
38. J. Mareš et al., Alternative biosynthetic starter units enhance the structural diversity of cyanobacterial lipopeptides. *Appl. Environ. Microbiol.* **85**, e02675-18 (2019).
39. N. A. Moss et al., Nature's combinatorial biosynthesis produces vatiamides A-F. *Angew. Chem. Int. Ed. Engl.* **58**, 9027–9031 (2019).
40. N. Eusébio et al., Discovery and heterologous expression of microginins from Microcystis aeruginosa LEGE 91341. *ACS Synth. Biol.* **11**, 3493–3503 (2022).
41. J. Moldenhauer, X.-H. Chen, R. Borriss, J. Piel, Biosynthesis of the antibiotic bacillaene, the product of a giant polyketide synthase complex of the trans-AT family. *Angew. Chem. Int. Ed. Engl.* **46**, 8195–8197 (2007).
42. R. F. Little, C. Hertweck, Chain release mechanisms in polyketide and non-ribosomal peptide biosynthesis. *Nat. Prod. Rep.* **39**, 163–205 (2021).
43. J. Young et al., Elucidation of gephyronic acid biosynthetic pathway revealed unexpected SAM-dependent methylations. *J. Nat. Prod.* **76**, 2269–2276 (2013).
44. R. Ratnayake et al., Dolastatin 15 from a marine cyanobacterium suppresses HIF-1α mediated cancer cell viability and vascularization. *ChemBioChem* **21**, 2356–2366 (2020), 10.1002/cbic.202000180.
45. H. Luesch, G. G. Harrigan, G. Goetz, F. D. Horgen, The cyanobacterial origin of potent anticancer agents originally isolated from sea hares. *Curr. Med. Chem.* **9**, 1791–1806 (2002).
46. H. Luesch et al., Symplostatin 3, a new dolastatin 10 analogue from the marine cyanobacterium *Symploca* sp. VP452. *J. Nat. Prod.* **65**, 16–20 (2002).
47. G. Lassiter et al., Belantamab mafodotin to treat multiple myeloma: A comprehensive review of disease, drug efficacy and side effects. *Curr. Oncol.* **28**, 640–660 (2021).
48. M. Z. Ansari, J. Sharma, R. S. Gokhale, D. Mohanty, In silico analysis of methyltransferase domains involved in biosynthesis of secondary metabolites. *BMC Bioinform.* **9**, 454 (2008).
49. J. Mareš et al., *Aetokthonos hydrillicola* Thurmond2011, whole genome shotgun sequencing project. NCBI GenBank. https://www.ncbi.nlm.nih.gov/nuccore/JAALHA000000000.2. Deposited 24 June 2022.
50. M. Schwark, T. H. J. Niedermeyer, Analytical data of Aetokthonostatins. Figshare. https://doi.org/10.6084/m9.figshare.22578616.v1. Deposited 3 September 2023.